International Journal of Nanomedicine

Dovepress
Taylor & Francis Group

Open Access Full Text Article

ORIGINAL RESEARCH

Engineering Multifunctional Nanozymes to Reprogram Oxidative Stress and Inflammation in Chronic Wounds

Qingyan Li[1,*], Weilin Zheng[2,*], Jingge Cheng[1,*], Bo Li[1], Yutian Lei[1], Huilong Guo[1], Youshan Xv[3], Jiaming Huang[4], Xiaoxing Liao[1,5]

[1]Emergency and Disaster Medicine center, The Seventh Affiliated Hospital of Sun Yat-Sen University, Shenzhen, Guangdong Province, People's Republic of China; [2]Department of Hepatobiliary and Gastrointestinal Surgery, The First Affiliated Hospital of Kunming Medical University, Kunming, Yunnan Province, People's Republic of China; [3]The Huiqiao Medical Center (International Medical Service) of Nanfang Hospital, Southern Medical University, Guangzhou, Guangdong Province, People's Republic of China; [4]Department of Hepatobiliary and Gastrointestinal Surgery, Shenzhen Guangming District People's Hospital, Shenzhen, Guangdong Province, People's Republic of China; [5]The Institute of Emergency Care and Resuscitation, The Seventh Affiliated Hospital of Sun Yat-Sen University, Shenzhen, Guangdong Province, People's Republic of China

*These authors contributed equally to this work

Correspondence: Xiaoxing Liao; Jiaming Huang, Email liaowens@163.com; huangjiaming@szgmrmyy.cn

Introduction: Diabetic wounds represent a growing clinical challenge worldwide, characterized by persistent immune dysregulation and excessive inflammation that lead to impaired healing and chronic progression.

Methods: To address this, we developed a composite nanosystem, termed Ru@ACEI, composed of ruthenium-incorporated hollow mesoporous silica nanoparticles loaded with angiotensin-converting enzyme inhibitors (ACEIs).

Results: The Ru@ACEI nanoparticles exhibit dual enzyme-mimetic activities (superoxide dismutase and catalase), effectively scavenging excess reactive oxygen species (ROS). This activity reduces cellular apoptosis and promotes endothelial cell proliferation. Following cellular uptake, Ru@ACEI catalyzes the decomposition of peroxides into water and oxygen, thereby suppressing the NLRP3/Caspase-3/Caspase-9 apoptosis pathway. The consequent improvement in endothelial cell survival helps reverse local hyperinflammation in diabetic wounds.

Conclusion: Collectively, these findings demonstrate that the Ru@ACEI nanosystem accelerates diabetic wound healing by mitigating the inflammatory microenvironment and downregulating the expression of pro-inflammatory factors, offering a promising therapeutic strategy for managing chronic diabetic wounds.

Keywords: diabetic wound, nanoenzyme, apoptosis, ROS-scavenge, anti-inflammatory microenvironment

Introduction

Diabetic wounds (DWs) represent a severe and prevalent complication of diabetes, often progressing into chronic ulcers that significantly impair quality of life and increase mortality risks.[1] Current clinical management relies on standard approaches including debridement, antimicrobial dressings, negative pressure wound therapy, and growth factor applications.[2] However, these conventional treatments often fail to adequately address the underlying pathological microenvironment—particularly persistent inflammation, excessive oxidative stress, and endothelial dysfunction[3]—highlighting a clear need for more targeted and multifunctional therapeutic strategies. The impaired healing process in DWs is characterized by elevated levels of reactive oxygen species (ROS) that disrupt cellular homeostasis. Hyperglycemia overwhelms endogenous antioxidant defenses, leading to sustained inflammation, extracellular matrix (ECM) degradation, and impaired angiogenesis.[4] This oxidative environment further promotes apoptosis of fibroblasts and keratinocytes while suppressing vascularization, forming a vicious cycle frequently exacerbated by secondary infections.[5,6]

Received: 8 June 2025
Accepted: 22 October 2025
Published: 27 October 2025

Conventional treatments often fail to adequately restore redox balance, underscoring an urgent need for innovative and targeted therapeutic strategies to modulate the pathological microenvironment of diabetic wounds.[7–9]

Recent advances in nanomedicine have introduced various promising platforms for diabetic wound management. For instance, metal-based nanoparticles such as ruthenium (Ru) have attracted attention due to their inherent enzyme-mimetic antioxidant, anti-inflammatory, and pro-proliferative properties.[10,11] Nevertheless, the clinical translation of Ru nanoparticles is often hampered by stability concerns, uncontrolled release, and suboptimal biodistribution.[12] In parallel, hydrogels with microenvironment-responsive properties have emerged as effective delivery systems for chronic wound treatment.[13,14] A representative study reported a responsive multifunctional hydrogel that emulates the healing cascade, showing promising outcomes in skin repair by dynamically interacting with wound signals.[15] Beyond these material innovations, pharmacological approaches such as angiotensin-converting enzyme inhibitors (ACEIs) have demonstrated cytoprotective benefits via renin-angiotensin system (RAS) modulation. ACEIs mitigate angiotensin II (Ang II)-induced oxidative stress and apoptosis through angiotensin II type 1 receptor (AT1R) suppression and phosphatidylinositol 3-kinase/protein kinase B (PI3K/Akt) activation[16,17]—a mechanism well-documented in cardiovascular contexts that may also support diabetic wound repair by enhancing stromal cell survival under oxidative duress.[18] Importantly, ACEIs have been shown to promote collagen deposition and angiogenesis through activation of protective signaling pathways,[19] suggesting their significant potential for diabetic wound repair. *The combination of Ru nanoparticles and ACEI offers a compelling synergistic rationale: the catalytic ROS-scavenging activity of Ru nanoparticles[20] directly mitigates the oxidative stress that impedes wound healing, while ACEI concurrently modulates RAS overactivation—a key pathway implicated in diabetic microvascular complications.[21] This dual approach simultaneously targets both oxidative and inflammatory pathways, thereby providing a more comprehensive mechanism for microenvironment remodeling.

Inspired by these developments, and to overcome the limitations of monomodality therapies, we engineered Ru@ACEI—a synergistic nanoplatform that combines the robust ROS-scavenging capacity of Ru nanoparticles with the cytoprotective and regenerative functions of an ACEI. This system leverages Ru-based catalase-like activity to decompose ROS and alleviate inflammation, while the ACEI coating not only improves nanoparticle stability and wound retention but also promotes endothelial migration and collagen deposition. Unlike conventional single-response systems, Ru@ACEI is designed to operate dual-responsively within the oxidative and proteolytic microenvironments of chronic wounds. It represents an integrated strategy targeting multiple pathological pathways concurrently, including ROS accumulation, persistent inflammation, aberrant angiogenesis, and stromal cell apoptosis. Through comprehensive in vitro and in vivo validation, we demonstrate that Ru@ACEI not only accelerates wound closure but also enhances vascular network regeneration and reduces cellular apoptosis. By synergistically reprogramming the hostile wound microenvironment, this multifunctional nanoplatform offers a novel and translatable therapeutic strategy against diabetic wound pathogenesis (Scheme 1).

Methods

Synthesis and Characterization of Ru@ACEI Nanoparticles

Nanoparticle Fabrication

The Ru@ACEI nanoconstruct was synthesized via a multi-step procedure. Monodisperse polystyrene (PS) microspheres (500 nm diameter) synthesized by emulsion polymerization served as sacrificial templates. These templates were incubated with 10 mM ruthenium(III) chloride solution ($RuCl_3 \cdot xH_2O$, Aladdin, China) under continuous stirring at 600 rpm (IKA RCT basic magnetic stirrer, Germany) for 12 h at 25 °C to adsorb Ru^{3+} ions. The Ru-loaded PS particles were collected by centrifugation at 10,000 rpm for 10 min (Centrifuge 5424 R, Eppendorf, Germany) and washed three times with deionized water. A mesoporous silica shell was then formed around the templates via a modified Stöber process. Briefly, 0.3 g CTAB (99%, Aladdin, China) and 1.5 mL TEOS (98%, Macklin, China) were added to the particle suspension under alkaline conditions (pH $\approx 10.5 \pm 0.5$, adjusted using 0.1 M NaOH) and reacted for 6 h at 60 °C. The resulting core–shell particles ($PS@Ru@SiO_2$) were calcined at 550 °C for 6 h (KSL-1100X muffle furnace, Hefei Kejing, China) to remove the PS core and CTAB template, yielding hollow mesoporous silica nanoparticles loaded with Ru nanoparticles (Ru-MSN). The Ru-MSN were functionalized with 2% (v/v) APTES (99%, Sigma-Aldrich, USA) in

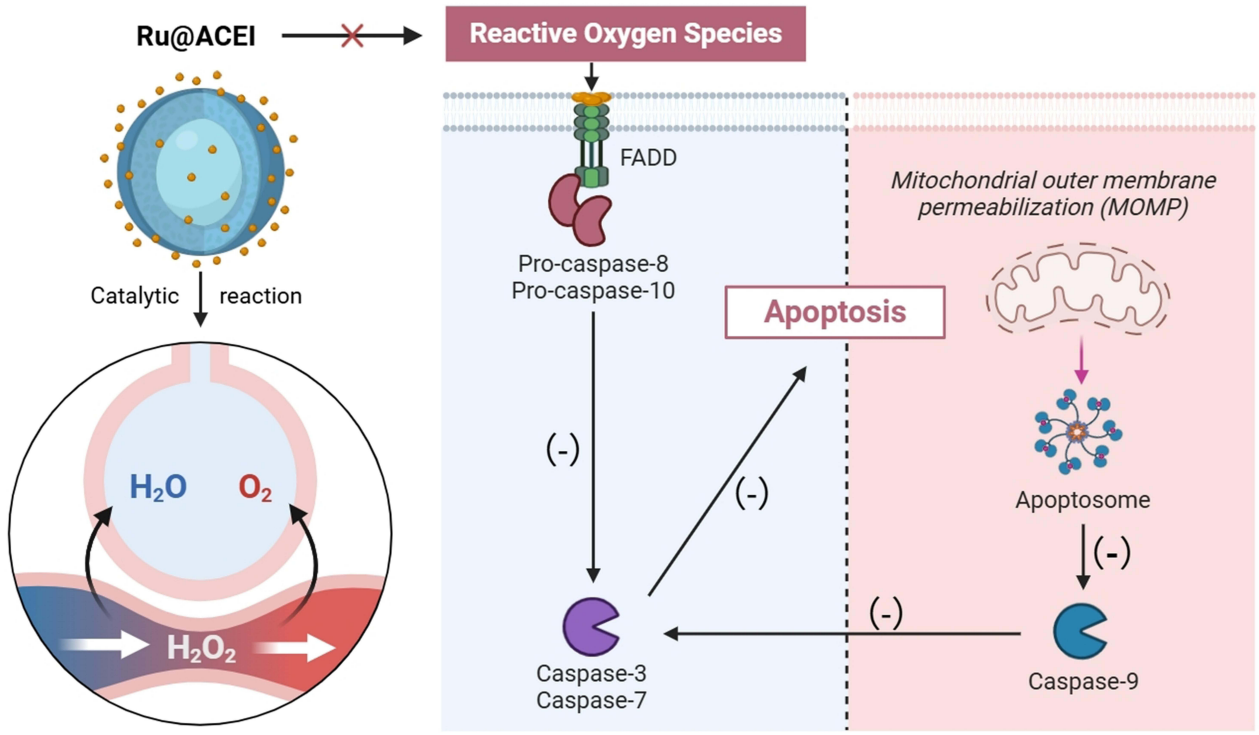

Scheme 1 Schematic of Ru@ACEI nanoparticles used for anti-inflammatory treatment.

ethanol for 4 h at 70 °C to introduce amine groups. For the ACEI component, enalapril maleate (MedChemExpress, USA) was selected as the model angiotensin-converting enzyme inhibitor. ACEI-loaded liposomes were prepared using the thin-film hydration method. HSPC (55 mol%), cholesterol (40 mol%), and enalapril maleate (5 mol%) were dissolved in chloroform, evaporated under reduced pressure at 40 °C (rotary evaporator RE-52AA, Yarong, China), and hydrated with PBS (pH 7.4) at 60 °C. The suspension was extruded 11 times through 100 nm polycarbonate membranes (Whatman, USA) using a mini-extruder (Avanti Polar Lipids, USA). The encapsulation efficiency of enalapril maleate was determined to be 88.2 ± 3.5% using HPLC (Agilent 1260 Infinity II) with a C18 column, using a mobile phase of acetonitrile/0.1% phosphoric acid (45:55, v/v) at 1.0 mL/min and detection at 215 nm. The final Ru@ACEI nanoparticles were formed by incubating laminated Ru-MSN with ACEI-liposomes (mass ratio 1:2) for 2 h at 25 °C under gentle agitation. The product was purified by centrifugation at 12,000 rpm for 15 min and stored in PBS at 4 °C.

Characterization

Morphology and microstructure were analyzed using TEM (JEM-2100F, JEOL, Japan) and HR-TEM with EDS mapping (X-MaxN 80, Oxford Instruments, UK). Samples were prepared on carbon-coated copper grids and air-dried. UV-Vis spectra were recorded using a Shimadzu UV-2600 spectrophotometer (Japan) with 1 cm path length quartz cuvettes. Hydrodynamic diameter and zeta potential were measured using a Zetasizer Nano ZS90 (Malvern Panalytical, UK) after dilution in PBS (for DLS) or 1 mM KCl (for zeta potential). All measurements were performed in triplicate.

CAT-Like Activity

For the UV-Vis spectrophotometric assay, the decomposition of H_2O_2 was monitored by measuring the decrease in absorbance at 240 nm over time using a UV-1800 spectrophotometer (Shimadzu, Japan) operated in kinetic mode at 25 °C. The reaction mixture contained 100 μg/mL Ru@ACEI and 10 mM H_2O_2 in phosphate-buffered saline (PBS, pH 7.4, room temperature), with a total volume of 2.5 mL. Measurements were taken every 30s for a total duration of 10 min. The catalytic activity was calculated based on the slope of the linear region of the time-dependent absorbance decrease. All assays were performed in triplicate. The CAT-like activity was further quantitatively determined using

https://doi.org/10.2147/IJN.S545569

a commercial Catalase Assay Kit (Beyotime Biotechnology, China, Cat. No. S0051) according to the manufacturer's instructions. Briefly, 30 μL of sample (100 μg/mL Ru@ACEI in PBS) was mixed with 30 μL of H_2O_2 substrate solution and incubated at room temperature for 5 min. The reaction was terminated by adding 30 μL of stop solution, followed by the addition of 30 μL of chromogenic agent. After incubation at room temperature for 15 min, the absorbance at 520 nm was measured using a SpectraMax M2e microplate reader (Molecular Devices, USA).[22] Additionally, the H_2O_2 elimination process was visually documented through digital imaging under consistent lighting conditions.[23]

Cell Culture and Treatment

The human keratinocyte cell line (HaCaT), human umbilical vein endothelial cells (HUVECs), and mouse fibroblast cell line (L929) were obtained from iCELL Bioscience Inc. (Shanghai, China). All cell lines were cultured in Dulbecco's Modified Eagle Medium (DMEM, Gibco, USA) supplemented with 10% fetal bovine serum (FBS, Gibco, USA) and maintained at 37 °C in a humidified incubator (HERAcell 150i, Thermo Scientific, USA) with 5% CO_2. For in vitro treatments, cells were exposed to 100 μg/mL of Ru@ACEI nanoparticles in phosphate-buffered saline (PBS) containing 100 μM H_2O_2.

Biosecurity Verification

The CCK-8 kit (BA00208, Bioss) was used to test the cytotoxicity of HUVEC, L929 and HaCaT cells treated with RuNp, ACEI and Ru@ACEI respectively. The proliferation ability of HUVEC cells was tested using LDH (M1020, Solarbio)[24] and MTT kits (BC0680, Solarbio)[25] according to the instructions. HUVEC cells were seeded at a density of 5×10^4 cells per well on a confocal microscope slide and cultured at 37°C, 5% CO_2 until 70% fusion. PBS (pH=7) and 100 μM H_2O_2[26] were added to the three groups, with the H_2O_2 group exposed to 100 μg/mL Ru@ACEI, RuNp, and ACEI. The medium was aspirated, and the cells were gently washed three times with pre-warmed PBS (1 min each time). The cells were then fixed in 4% PFA at room temperature for 15 min, followed by three PBS washes. A 0.1% Triton X-100 solution (prepared in PBS) was added and incubated at room temperature for 10 min, followed by three PBS washes. The cells were blocked in 1% BSA (prepared in PBS with 0.1% Tween-20) at room temperature for 30 min to reduce non-specific binding. Phalloidin (Alexa Fluorescence 488-labeled; ab143532, Abcam) working solution (diluted 1:100–1:200 in PBS) was added under light protection and incubated at room temperature for 30–60 min. The cells were washed three times with PBS (5 min each time). DAPI (1 μg/mL, prepared in PBS; D-9106, Bioss) was added and incubated for 5 min, followed by a PBS wash. Images were captured using a Zeiss LSM 880 confocal microscope (Carl Zeiss, Germany) under the appropriate immunofluorescence channels.

In vitro ROS Detection

In vitro ROS detection was carried out to evaluate intracellular reactive oxygen species levels in HUVEC cells using a commercial ROS assay kit (50101ES01, Yeason, China). Following the manufacturer's protocol, cells from different treatment groups—including control, H_2O_2, H_2O_2 + RuNp, H_2O_2 + ACEI, and H_2O_2 + Ru@ACEI—were incubated for 48 hours. Subsequently, the fluorescent probe DCFH-DA (for cytosolic ROS) and MitoSOX™ Red mitochondrial superoxide indicator (for mitochondrial ROS) were diluted in serum-free medium, applied to the cell suspensions, and incubated at 37 °C in the dark for 30 minutes. After staining, the cells were washed gently with PBS to remove excess probe. Fluorescence images were acquired using an inverted fluorescence microscope (model IX73, Olympus, Japan) equipped with a FITC filter set (excitation/emission = 498/530 nm) under ×200 magnification.[27]

Construction of in vivo Wound Model

A streptozotocin (STZ)-induced type 1 diabetic mouse model was established as previously described[28] with modifications. Briefly, eight-week-old male BALB/c mice (n = 40) were purchased from Vital River Laboratory Animal Technology Co., Ltd. (Beijing, China) and acclimatized for one week under specific pathogen-free (SPF) conditions at 22 ± 2 °C with a 12 h light/dark cycle. After fasting for 6 h, diabetes was induced by intraperitoneal injection of STZ (Sigma-Aldrich, USA; 55 mg/kg/day, dissolved in 0.05 M citrate buffer, pH 4.5) for five consecutive days. Age-matched control mice received citrate buffer only. Blood glucose levels were measured using a glucometer (Accu-Chek Performa,

Roche, Germany) via tail vein sampling. Mice with non-fasting blood glucose levels ≥ 16.7 mmol/L (300 mg/dL) for three consecutive days were considered diabetic and included in the study. One week after diabetes confirmation, mice were anesthetized with isoflurane (4% for induction, 2% for maintenance), and the dorsal hair was shaved and disinfected with povidone-iodine. Two full-thickness excisional wounds (15 mm in diameter) were created on the dorsum using sterile surgical scissors and forceps. Mice were randomly assigned to five experimental groups (n = 8 per group) using a computer-generated randomization list: (1) non-diabetic control; (2) diabetic control (saline-treated); (3) diabetic + RuNP; (4) diabetic + ACEI; (5) diabetic + Ru@ACEI. Researchers performing wound measurements and histological analyses were blinded to group assignments throughout the experiment. Wound areas were measured every three days using a digital caliper and photographed under standardized conditions.

Histological and Immunofluorescence Staining

Histological examination of diabetic wounds was conducted through hematoxylin and eosin (H&E) staining. Tissue samples from the grafted area were first fixed in 10% formalin solution (Sigma-Aldrich, Ireland), followed by dehydration using ethanol and embedding in paraffin. The embedded tissues were then sectioned into 5 μm thick slices with a Leica RM2255 microtome. After dewaxing and rehydration, H&E staining (C0105S, Beyotime) and IL-1β staining (ab283818, Abcam) were performed in accordance with the manufacturer's guidelines.[29,30] Imaging was carried out with a Nikon ECLIPSE 90i light microscope (Nikon, Tokyo, Japan).

For the assessment of inflammation in diabetic wounds, immunofluorescence staining was employed. The tissue sections underwent deparaffinization, dehydration through an alcohol gradient, and antigen retrieval. After blocking with 10% BSA, the sections were incubated overnight at 4°C with anti-mouse ROS antibody (H131224, Aladdin). Images were acquired using a confocal laser scanning microscope (CLSM) following DAPI staining.

Masson's Trichrome Staining

Masson's trichrome staining was conducted to assess collagen deposition in wound tissues. Deparaffinized and rehydrated sections (5 μm) were first treated with Bouin's solution (56 °C, 1 h), rinsed, and stained with Weigert's hematoxylin (10 min). After differentiation in 1% acid alcohol, sections were incubated in Biebrich scarlet-acid fuchsin (10 min) and phosphomolybdic–phosphotungstic acid (10 min), followed by aniline blue staining (5 min) to highlight collagen. Sections were then dehydrated, cleared, and mounted. Imaging was performed using a Nikon Eclipse Ni-U microscope, and collagen content was quantified with ImageJ (v1.53) by measuring the blue-stained area percentage across five random fields per sample.

RNA Isolation and Quantitative Real-Time PCR

To evaluate the inflammatory responses in HUVECs, quantitative real-time polymerase chain reaction (qPCR) was performed to measure the expression levels of key inflammatory mediators, including NLRP3, Caspase3, Caspase9, IFN-γ, and IL-10. Total RNA was extracted using the AllPrep DNA/RNA Mini Kit (Qiagen, Germany). Complementary DNA (cDNA) was synthesized from 1 μg of total RNA using the SuperScript™ VILO™ cDNA Synthesis Kit (Thermo Fisher Scientific, USA).[31] qPCR amplification was carried out on a CFX96 Touch Real-Time PCR Detection System (Bio-Rad, USA) with SYBR Green chemistry. Each reaction was performed in triplicate under the following cycling conditions: initial denaturation at 95 °C for 2 min, followed by 40 cycles of 95 °C for 15s and 60 °C for 30s. The comparative threshold cycle (CT) method (2^(-ΔΔCT)) was used for quantification of relative gene expression, with GAPDH serving as the internal reference gene. All primer sequences (listed in Table 1) were designed using NCBI Primer-BLAST and synthesized by Integrated DNA Technologies (USA).

ELISA Assay

Enzyme-linked immunosorbent assay (ELISA) was performed to quantify the levels of key pro-angiogenic and inflammatory factors, including procalcitonin (PCT; P771070, Macklin, China), C-reactive protein (CRP; C774624-48T, Macklin, China), and interleukin-1β (IL-1β; AF5103, Affinite, China), in accordance with the manufacturers'

Table 1 Sequences of Primers Used in Quantitative Polymerase Chain Reaction

Gene	Forward 5' - 3'	Reverse 5' - 3'
NLRP3	*TTGCTGCCATCTCTGGTTTG*	*AGCCTGGATCTTGTTGGGATG*
IL-10	*GACTTTAAGGGTTACCTGGGTTG*	*TCACATGCGCCTTGATGTCTG*
Caspase3	*CATGGAAGCGAATCAATGGACT*	*CTGTACCAGACCGAGATGTCA*
IFN-γ	*ACTTGAATGTCCAACGCAA*	*CGAAACAGCATCTGACTCC*
Caspase9	*CTTCGTTTCTGCGAACTCACAG*	*GCATTTCCCCTCAAACTCTCAA*

instructions. Absorbance readings were measured at 450 nm using a SpectraMax M2e microplate reader (Molecular Devices, USA).

Western Blot

Western blot analysis was performed to evaluate protein expression levels. Total protein concentrations were determined using a BCA protein assay kit (23225, Thermo Fisher Scientific, USA). Proteins were separated by electrophoresis on 10% SDS-polyacrylamide gels and subsequently transferred onto PVDF membranes (0.45 μm, Millipore, USA). The membranes were blocked with 5% bovine serum albumin (BSA, prepared in TBST) for 1 h at room temperature and then incubated overnight at 4 °C with the following primary antibodies: anti-rabbit IL-1β (1:2000; ab283818, Abcam, UK), Caspase3 (1:2000; ab32351, Abcam, UK), NLRP3 (1:2000; ab263899, Abcam, UK), and β-actin (1:20000; ab9485, Abcam, UK). After washing three times with TBST, the membranes were incubated with a horseradish peroxidase (HRP)-conjugated goat anti-rabbit secondary antibody (1:3000; ab6721, Abcam, UK) for 1 h at room temperature. Protein bands were visualized using a ChemiDoc™ MP Imaging System (Bio-Rad, USA) with an enhanced chemiluminescence (ECL) detection reagent (32106, Thermo Fisher Scientific, USA).

Statistical Analysis

All data are expressed as mean ± SD. Statistical analyses were performed using GraphPad Prism software. Intergroup comparisons were conducted as follows: Two-group comparisons: Unpaired Student's *t*-test; Multi-group comparisons: One-way ANOVA with Tukey's post hoc test. A threshold of $p < 0.05$ was considered statistically significant.

Results and Discussion

Design and Characterization of Ru@ACEI

In this study, we synthesized and characterized Ru@ACEI for its potential therapeutic applications in wound healing and antioxidant activity. The material fabrication process and the structural characteristics of Ru@ACEI were systematically evaluated. As shown in Figure 1A, a schematic illustration outlines the construction of Ru@ACEI, where Ru nanoparticles (RuNps) are encapsulated within ACEI. The TEM images reveal the morphology of RuNps and the encapsulated Ru@ACEI (Figure 1B), confirming the uniform size and dispersion of the nanoparticles. At the same time, Ru-MSN particles were coated with ACEI liposomes on the outer layer (Figure 1B, yellow arrow). High-resolution TEM (HR-TEM) analysis and corresponding EDS elemental mapping demonstrate the successful incorporation of Ru nanoparticles into ACEI, with clear evidence of Ru distribution in the composite (Figure 1C). Furthermore, the UV-visible absorption spectrum showed that both ACEI and Ru@ACEI had characteristic absorption peaks at 257 nm, indicating that Ru@ACEI successfully encapsulated ACEI (Figure 1D). DLS analysis in Figure 1E provides insights into the hydrodynamic diameter distribution of the nanoparticles (Ru@ACEI: ~228 nm, RuNp: ~199 nm), which is consistent with the size observed in TEM images. The ζ potential analysis shows that although the Np surface changes from positive charge

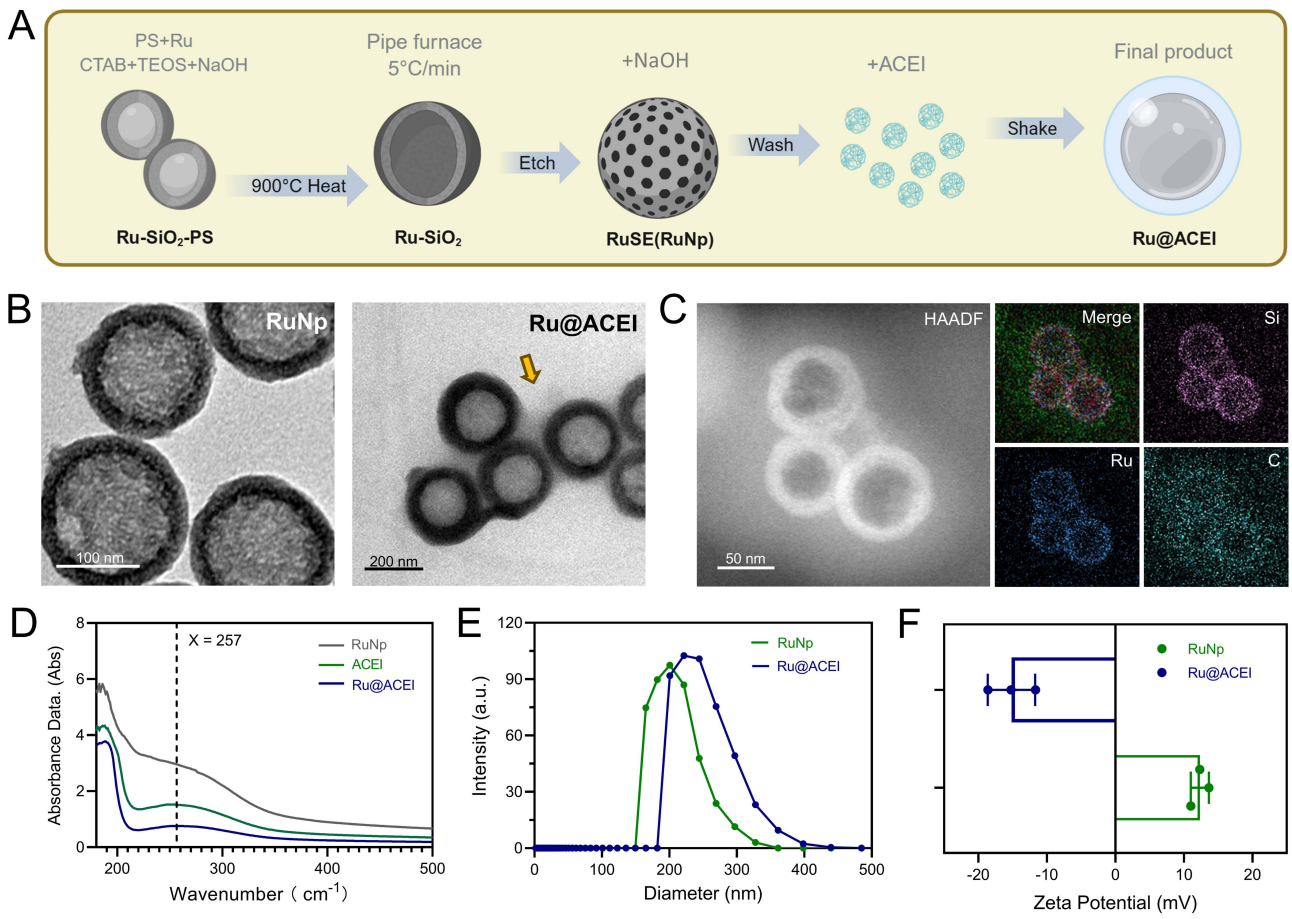

Figure 1 Material fabrication and characterization. (**A**) Schematic illustration of Ru@ACEI construction. (**B**) TEM images of Ru nanoparticles (RuNps) and Ru@ACEI; Yellow arrow: ACEI envelope surrounding RuNp. (**C**) HR-TEM image and corresponding EDS elemental mapping of Ru@ACEI. (**D**) UV-vis absorption spectra of RuNps, ACEI, and Ru@ACEI. (**E**) Hydrodynamic diameter distribution of RuNps and Ru@ACEI measured by DLS. (**F**) Zeta potential analysis of RuNps and Ru@ACEI.

to negative charge after ACEI loading,[32] the Ru@ACEI surface still maintains a stable charge state like RuNp, ensuring good colloid stability (Figure 1F).

Catalytic Activity and Biosafety of Ru@ACEIs

The goal of constructing Ru@ACEI was to achieve anti-inflammatory effects through efficient ROS elimination, and thus its catalytic antioxidant activity was thoroughly investigated. Figure 2A illustrates the mechanism of reactive oxygen species (ROS) clearance by Ru@ACEI. TEM observations revealed that the structural integrity of Ru@ACEI was progressively compromised under H_2O_2 treatment (Figure 2B), mimicking the oxidative conditions of an inflammatory microenvironment. This controlled degradation behavior is crucial for regulating the release of encapsulated therapeutic components (eg, Ru ions and ACEI), thereby promoting site-specific drug delivery and minimizing potential off-target effects. Notably, Ru@ACEI exhibited H_2O_2 scavenging efficiency comparable to RuNps alone (Figure 2C), indicating that the ACEI loading did not impair the intrinsic antioxidant capacity of the ruthenium nanoparticles. Quantitative analysis using a Catalase Assay Kit showed that the catalase-like activity of RuNps and Ru@ACEI further confirming their high and equivalent antioxidant activities (Figure 2D). The absence of enhanced catalytic activity after ACEI loading can be mechanistically explained by the distinct roles of the two components: while RuNps primarily function as catalytic ROS scavengers, ACEI exerts its therapeutic effects through pharmacological regulation of the renin-angiotensin system (RAS), particularly by attenuating angiotensin II-mediated oxidative stress and inflammation via AT1R suppression and PI3K/Akt activation. Thus, the synergy between RuNps and ACEI is not manifested through augmented catalytic activity, but rather through complementary mechanisms—where RuNps mitigate extracellular and

https://doi.org/10.2147/IJN.S545569

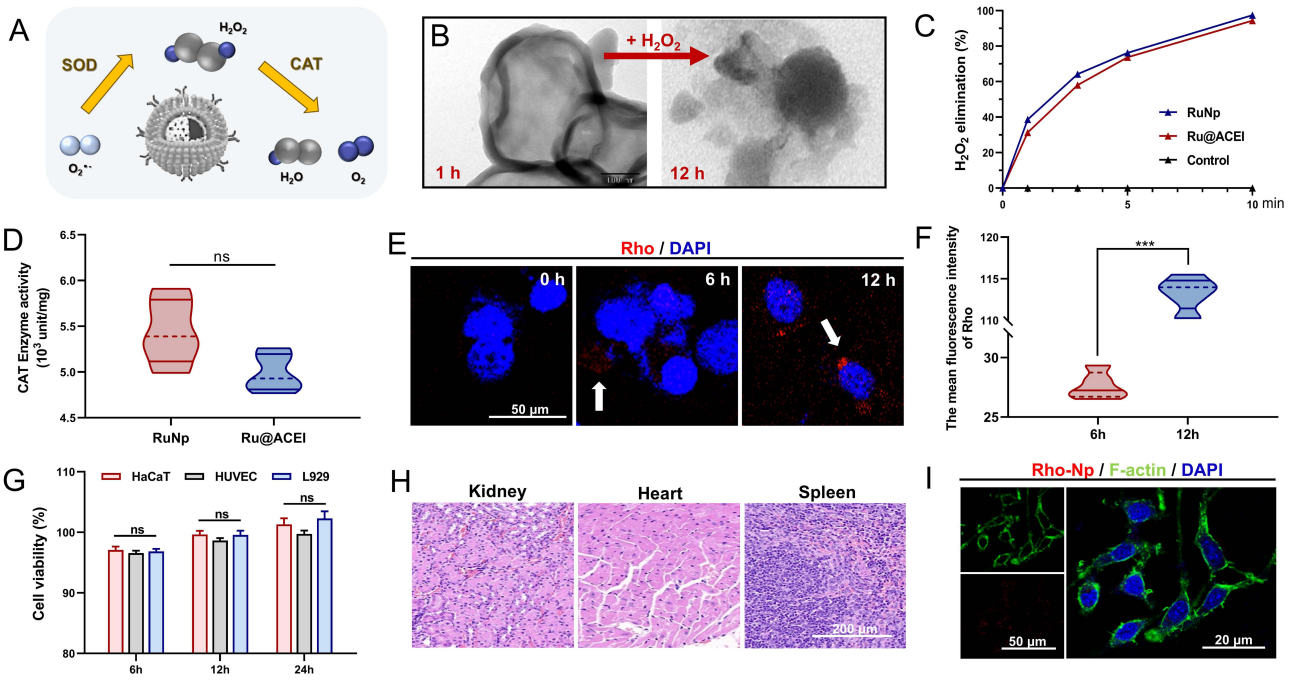

Figure 2 CAT and SOD-like activities of Ru@ACEI. (**A**) Schematic illustration of ROS clearance by Ru@ACEI. (**B**) TEM visualization of Ru@ACEI post-exposure to an aqueous 5% H_2O_2 solution. (**C**) H_2O_2 scavenging efficiency of RuNps and Ru@ACEI. (**D**) CAT-like activity of RuNps and Ru@ACEI quantified by ELISA. (**E**) Cellular uptake of Rho-labeled Ru@ACEI by endothelial cells after co-culture; White arrow: Ru@ACEI with intracellular Rho labeling. (**F**) Quantitative analysis of (**E**). (**G**) Cytotoxicity assessment of 100 μg/mL Ru@ACEI on dermal cell lines via CCK-8 assay. (**H**) H&E staining of major organs after topical application of 100 μg/mL Ru@ACEI for 3 days. (**I**) Morphological changes of endothelial cells post Ru@ACEI co-culture. Error bars indicate the mean ± standard deviation, n = 3, ns = no significant and ***$p < 0.001$.

intracellular ROS bursts, and ACEI concurrently modulates downstream inflammatory signaling and promotes cell survival. This dual-pathway intervention represents a novel therapeutic strategy that simultaneously targets both the initiators (ROS) and propagators (inflammatory responses) of diabetic wound pathology.

Cellular uptake studies demonstrated efficient internalization of Rho-labeled Ru@ACEI by endothelial cells (Figure 2E and F), supporting its potential for targeted intracellular delivery of both ROS-scavenging and anti-inflammatory components. The biosafety of nanoparticles is paramount for clinical translation, as their unique physicochemical properties may induce unintended biological effects. Key concerns include long-term accumulation, inflammatory responses, and potential cytotoxicity. Rigorous evaluation of hemocompatibility, organ clearance pathways, and off-target effects through standardized assays is essential. In this study, Ru@ACEI exhibited excellent biocompatibility in vitro. No significant cytotoxicity was observed in dermal cell lines (HUVEC, L929, HaCaT) after 48-hour exposure to 100 μg/mL Ru@ACEI (Figure 2G). Furthermore, no morphological abnormalities were observed in HUVECs co-cultured with Rho-labeled Ru@ACEI, with cells maintaining normal spreading and proliferation (Figure 2I). In vivo safety assessment showed that after 3 days of wound application, H&E staining of major organs (heart, liver, spleen, lung, and kidney) from mice treated with Ru@ACEI revealed no apparent pathological abnormalities or signs of acute toxicity (Figure 2H). These results confirm the favorable short-term safety profile of Ru@ACEI. However, we acknowledge that the current study has limitations regarding comprehensive safety evaluation. While our results demonstrate excellent acute biocompatibility, long-term toxicity assessments (beyond 72 hours) and detailed biodistribution studies were not conducted. These aspects represent important considerations for clinical translation that should be addressed in future investigations. Subsequent studies should include repeated-dose toxicity evaluations in diabetic models over extended periods (eg, 28 days) and employ techniques such as ICP-MS or fluorescence imaging to quantify nanoparticle accumulation in major organs. Despite these limitations, our Ru@ACEI design demonstrates a promising safety-optimized nanotherapeutic strategy by combining ROS-scavenging efficacy with ACEI-derived cytoprotection, showing >90% cell viability in vitro and negligible acute hepatotoxicity in vivo. The favorable preliminary safety profile, coupled

with the demonstrated therapeutic efficacy, supports further development of this novel approach for diabetic wound management.

To evaluate the practical applicability of Ru@ACEI for wound healing, we investigated its stability under physiological conditions. Ru@ACEI maintained excellent colloidal stability in both simulated wound fluid and DMEM supplemented with 10% FBS over 72 hours, with minimal changes in hydrodynamic diameter (Figure S1A) and zeta potential (Figure S1B). Importantly, the catalase-like activity was well preserved after 48-hour incubation in physiological media, retaining its initial CAT capacity (Figure S1C). These results demonstrate that Ru@ACEI maintains structural integrity and catalytic functionality in biologically relevant environments, supporting its potential for practical wound healing applications.

Ru@ACEI Improves Endothelial Cell Proliferation and Reduces Inflammatory Infiltration via ROS Scavenging

To assess the therapeutic effects of Ru@ACEI in oxidative stress-induced endothelial cell injury, we performed a series of functional and molecular assays. Endothelial cells exposed to H_2O_2 exhibited markedly reduced proliferation, which was significantly rescued by Ru@ACEI treatment, as demonstrated by EdU incorporation assays (Figure 3A and B). Reactive oxygen species (ROS) play a critical role in regulating endothelial cell proliferation through redox-dependent signaling.[33,34] Under diabetic conditions, hyperglycemia-induced pathological ROS overload causes oxidative damage to cellular components and leads to cell cycle arrest.[35] Furthermore, excessive ROS impair nitric oxide bioavailability, hindering endothelial migration and angiogenic function.[36] Consistent with these mechanisms, intracellular ROS levels were significantly reduced in the Ru@ACEI-treated group compared to other treatments (Figure 3C and D), underscoring its potent antioxidative capacity. Cytotoxicity assessments, including LDH release (Figure 3E) and MTT assays (Figure 3F), confirmed that Ru@ACEI significantly enhances cell viability under oxidative stress.

At the molecular level, Ru@ACEI treatment markedly downregulated the expression of apoptosis-related proteins and the pro-inflammatory cytokine IL-1β (Figure 3G and H). Quantitative real-time PCR analysis revealed that Ru@ACEI significantly suppressed the expression of key mediators of apoptosis and inflammation, with fold changes of –0.84 for NLRP3, –0.81 for Caspase-1, and –0.82 for Caspase-9 compared to the H_2O_2-treated group ($p < 0.01$). Western blot analysis further corroborated these findings, showing substantial reduction in NLRP3, cleaved Caspase-3, and IL-1β protein levels (Figure 3I and J). Collectively, these data demonstrate that Ru@ACEI restores ROS homeostasis, attenuates oxidative stress-induced apoptosis and inflammation, and promotes endothelial cell proliferation under pathological conditions. The enhanced proliferative recovery of HUVECs in a peroxidative microenvironment underscores the therapeutic potential of Ru@ACEI in mitigating diabetic endothelial dysfunction.

In vivo Anti-Inflammatory Effect and Promoting Wound Repair

In view of the promising in vitro performance, we further evaluated the anti-inflammatory and wound healing efficacy of Ru@ACEI in a streptozotocin (STZ)-induced type 1 diabetic mouse model. Full-thickness excisional wounds (15 mm diameter) were created on the dorsum of mice and treated regularly with 100 μg/mL Ru@ACEI or control formulations. As shown in Figure 4A, Ru@ACEI treatment significantly accelerated wound healing compared to other groups. Representative photographs (Figure 4B) and quantitative analysis of time to complete wound closure (Figure 4C) confirmed that Ru@ACEI-treated mice exhibited the most rapid healing, with average healing times of 21.97, 15.83, 16.10, and 13.87 days for the Sham, ACEI, RuNp, and Ru@ACEI groups, respectively. While both ACEI and RuNp monotherapies significantly improved healing compared to Sham controls, no statistically significant difference was observed between these two groups in terms of wound closure rate. However, comprehensive analysis revealed that the primary therapeutic advantage of Ru@ACEI extends beyond accelerated epithelialization. Heatmap analysis of wound healing progression (Figure 4D) and quantification of systemic inflammatory markers (Figure 4E and F) demonstrated that Ru@ACEI uniquely provides robust systemic anti-inflammatory effects in addition to local wound healing benefits. Notably, Ru@ACEI treatment resulted in remarkable 92.57% and 94.12% reductions in peripheral procalcitonin (PCT) and C-reactive protein (CRP) levels, respectively, compared to untreated controls. This substantial attenuation of systemic inflammation suggests that the combination therapy effectively breaks the vicious cycle of chronic inflammation

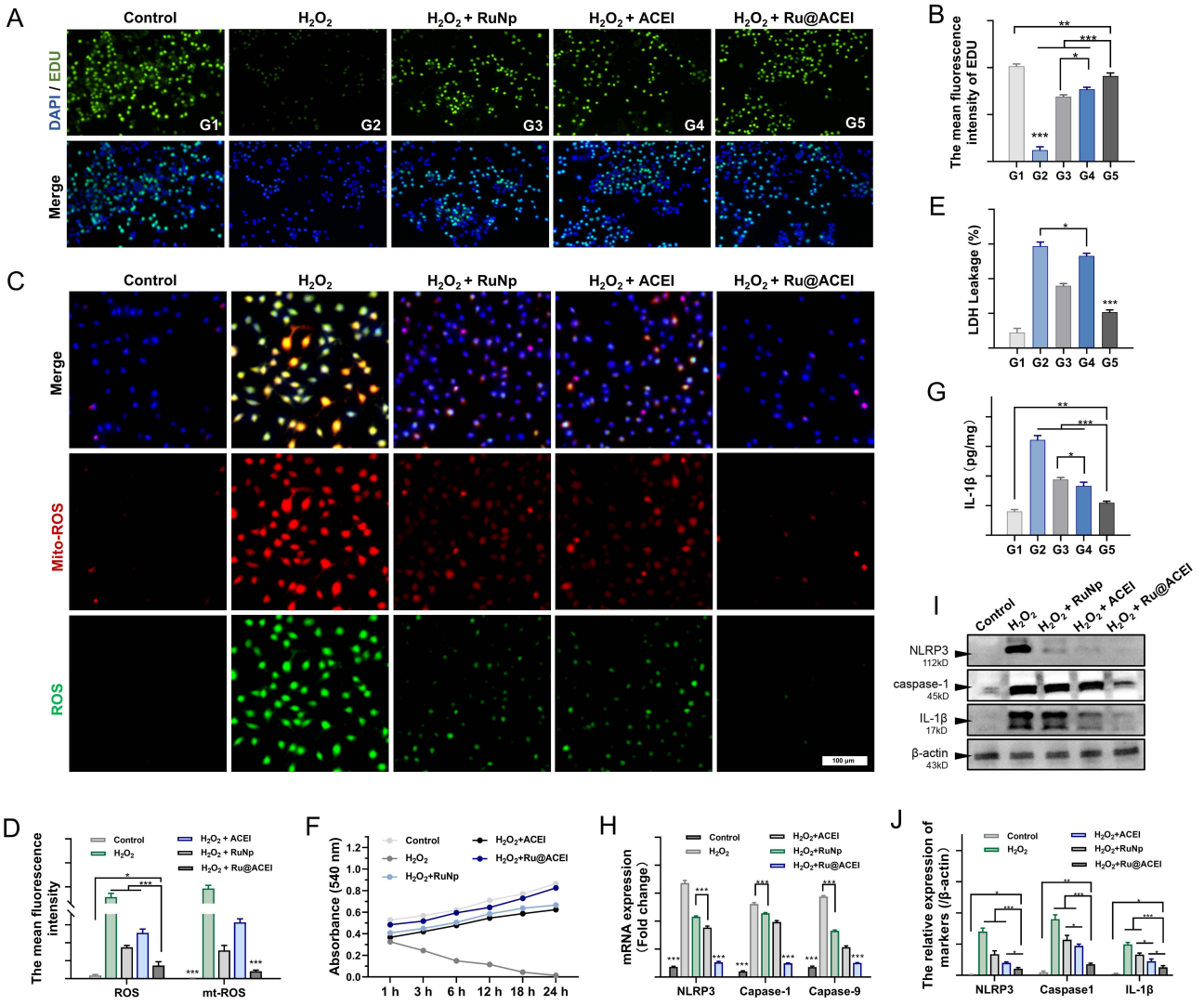

Figure 3 Ru@ACEI improves endothelial cell microenvironment through antioxidant effects. (**A**) Proliferation capacity of endothelial cells co-cultured with H_2O_2 in different treatment groups, assessed by EdU assay, and (**B**) its Quantitative analysis. (**C**) Intracellular ROS and mito-ROS levels detected by DCFH-DA and MitoSOX™ Red probe across treatment groups. (**D**) Corresponding quantitative analysis of ROS and mito-ROS levels. (**E**) Cytotoxicity evaluation of endothelial cells in different groups via LDH release assay. (**F**) Cell proliferation activity under oxidative stress conditions measured by MTT assay. (**G**) IL-1β secretion levels in supernatant quantified by ELISA. (**H**) Expression levels of apoptosis-related proteins in endothelial cells under oxidative microenvironment. (**I**) Western blotting assay of Pyroptosis, and (**J**) its relative analysis. Error bars represent mean ± SD (n=3); *p < 0.05, **p < 0.01, ***p < 0.001.

characteristic of diabetic wounds. In addition, Masson staining also observed that Ru@ACEI significantly improved collagen reconstruction, which is of great significance for improving scar formation in later stages (Figure 4G and H). The comparable wound closure rates but differential anti-inflammatory effects between monotherapies and the combination indicate that Ru@ACEI's superior efficacy may stem from its comprehensive modulation of the wound microenvironment—simultaneously addressing local oxidative stress through RuNp's catalytic activity and systemic inflammation through ACEI's pharmacological action—rather than solely accelerating physical wound closure. These findings position Ru@ACEI as a multifaceted therapeutic strategy that targets both local and systemic aspects of diabetic wound pathogenesis, offering a more complete approach to managing this complex condition.

Finally, Ru@ACEI's effects on apoptosis and inflammation were further explored at the molecular level. Immunofluorescence staining of ROS levels in skin tissues from wound sites (Figure 5A and B) and IHC quantification of IL-1β-positive cells (Figure 5C and D) revealed that Ru@ACEI effectively reduced ROS accumulation and inflammatory responses. qPCR analysis demonstrated that Ru@ACEI treatment significantly downregulated the expression of key pro-

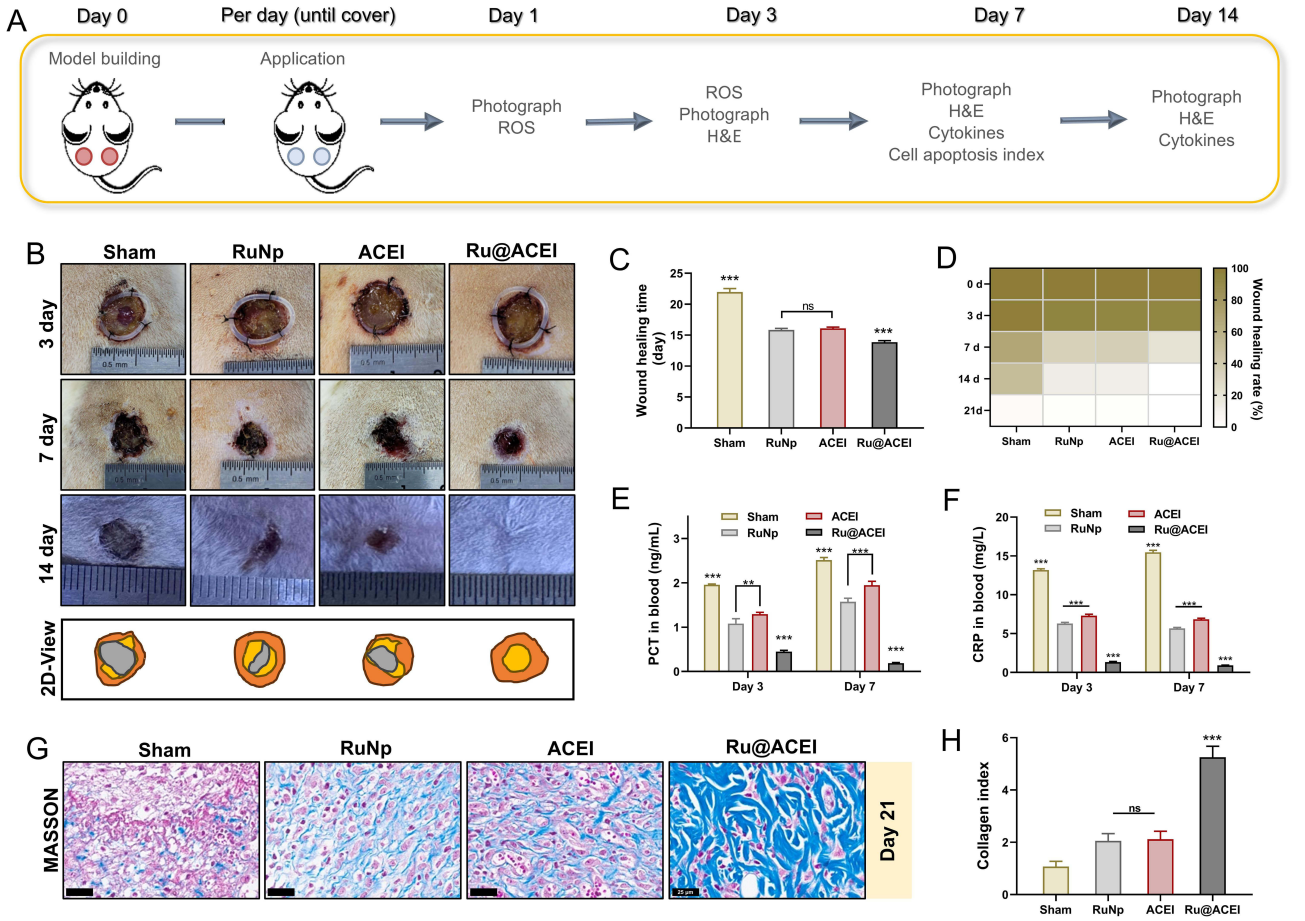

Figure 4 Ru@ACEI accelerates wound healing in vivo. (**A**) Schematic diagram of the animal experiment. (**B**) Representative photographs of wounds from different treatment groups. (**C**) Time required to achieve complete wound closure across four treatment groups. (**D**) Heatmap analysis of wound healing rates among groups. (**E**) Serum CRP levels and (**F**) PCT levels in treated mice at predetermined time points. (**G**) Masson staining and (**H**) related collagen index. Error bars represent mean ± SD (n=3); ns = no significant, **p < 0.01 and ***p < 0.001.

apoptotic and inflammatory genes, with reduce-fold changes relative to the diabetic control group of 0.76-fold for NLRP3 ($p < 0.01$), 0.80-fold for Caspase-3 ($p < 0.01$), and 0.72-fold for Caspase-9 ($p < 0.01$) (Figure 5E). These quantitative gene expression results provide clear evidence of Ru@ACEI's suppressive effects on pyroptotic and apoptotic pathways. Furthermore, Western blot analysis of NLRP3, Caspase-3, and IL-1β protein levels (Figure 5H and I) corroborated the transcriptional regulation observed in qPCR, confirming the inhibition of these pathways at the protein level. Ru@ACEI also modulated immune responses by significantly upregulating the anti-inflammatory cytokine IL-10 and downregulating the pro-inflammatory cytokine IFN-γ (Figure 5F and G). These findings indicate that Ru@ACEI enhances wound healing through multi-faceted anti-apoptotic and immunomodulatory mechanisms, effectively reducing pro-inflammatory signals while promoting anti-inflammatory responses. The results collectively demonstrate that Ru@ACEI exhibits significant antioxidant, anti-inflammatory, and tissue-regenerative effects, positioning it as a promising candidate for therapeutic applications in oxidative stress-related disorders and impaired wound healing.

Conclusion

In summary, we developed Ru@ACEI, a multifunctional nanoplatform that integrates reactive oxygen species (ROS) scavenging with diabetic wound microenvironment reprogramming. The design combines a catalytic ruthenium-based nanocarrier with an angiotensin-converting enzyme inhibitor (ACEI) surface coating, enabling dual-pathway therapy against oxidative stress and apoptosis. The hollow mesoporous silica framework incorporated with ruthenium nanoparticles efficiently decomposes hydrogen peroxide into water and oxygen, thereby alleviating ROS burst. Simultaneously,

https://doi.org/10.2147/IJN.S545569

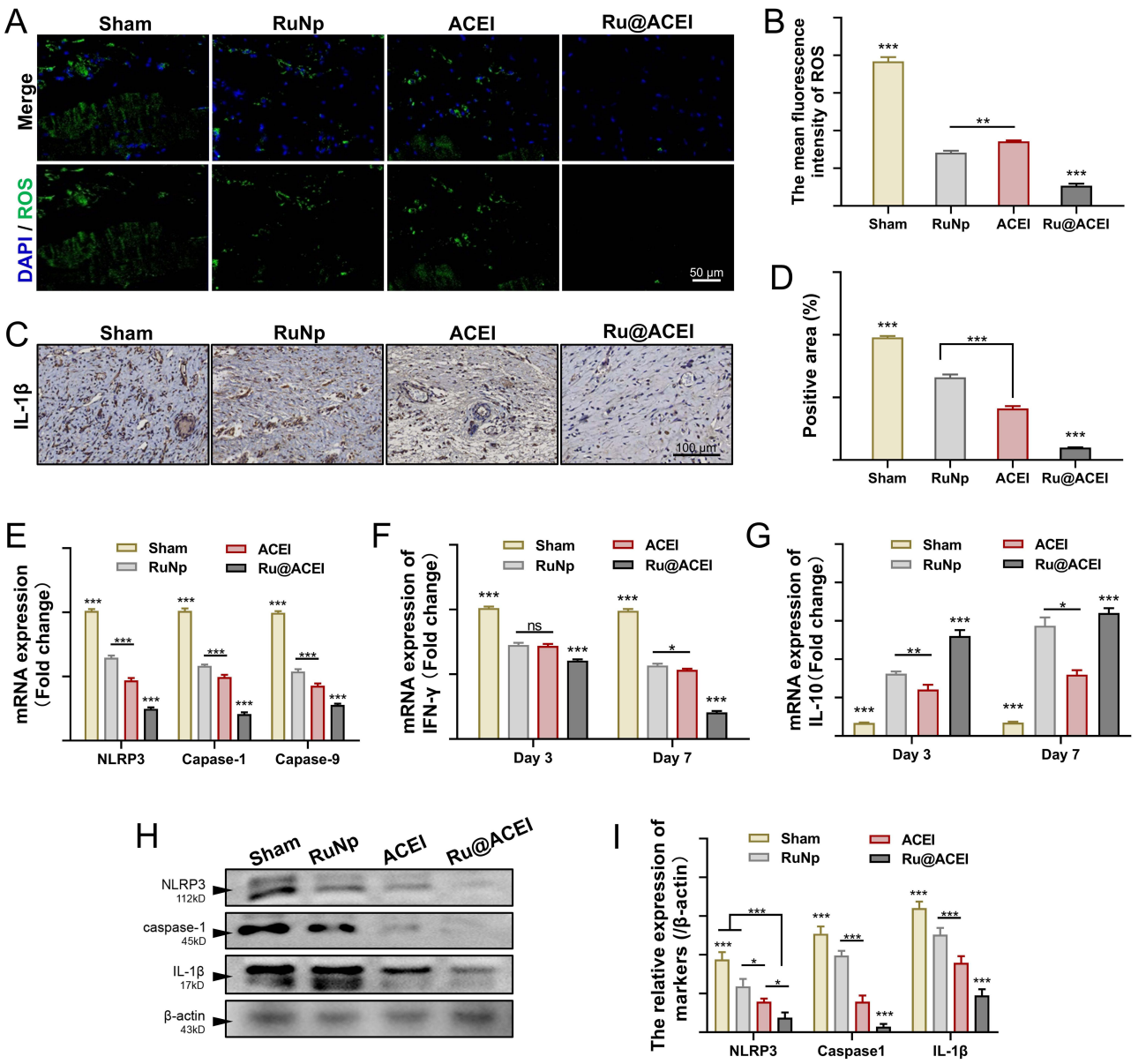

Figure 5 Ru@ACEI attenuates apoptosis pathways and modulates inflammatory factor expression to enhance immunoregulation in vivo. (**A**) ROS levels in skin tissues isolated from wounds of Sham-, RuNp-, ACEI-, and Ru@ACEI-treated mice, analyzed by immunofluorescence staining, and (**B**) its quantitative analysis; Green color indicates the ROS-positive. (**C** and **D**) IHC quantification of IL-1β-positive cells in wound tissues across groups. (**E**) Transcriptional levels of NLRP3/caspase signaling pathway components. qPCR analysis of (**F**) pro-inflammatory (IFN-γ) and (**G**) anti-inflammatory (IL-10) cytokine transcripts in wound tissues. (**H** and **I**) Western blotting assay of Pyroptosis, and their relative analysis. n = 3 samples/group and data are presented as mean ± SD. ns = no significant, ***p < 0.001, **p < 0.01 and *p < 0.05.

the ACEI layer—functioning as both a therapeutic agent and stabilizer—is released in response to the proteolytic wound microenvironment, where it attenuates NLRP3/caspase-mediated apoptotic signaling in endothelial cells. This combined action reduces pro-inflammatory cytokine secretion and promotes cellular proliferation and angiogenesis, resulting in improved anti-inflammatory and regenerative outcomes in diabetic wound models. While Ru@ACEI demonstrates compelling therapeutic potential, we acknowledge several translational challenges that must be addressed before clinical application, including scaling up synthesis while maintaining batch-to-batch consistency, evaluating long-term biosafety and biodistribution profiles, assessing cost-effectiveness relative to existing therapies, and navigating regulatory requirements for combination nanotherapeutics. Future studies will focus on optimizing manufacturing processes, conducting Good Laboratory Practice (GLP)-compliant toxicology studies, and validating efficacy in more complex diabetic wound models. Beyond diabetic wound healing, the antioxidant and anti-inflammatory mechanisms of Ru@ACEI suggest

potential applications in other ROS-related disorders, such as cardiovascular diseases (eg, atherosclerosis, myocardial ischemia-reperfusion injury), neurodegenerative conditions, and other chronic inflammatory disorders where redox imbalance plays a key pathogenic role. Despite these challenges, our findings provide proof-of-concept that convergently targeting oxidative stress and dysregulated apoptosis within a single nanoconstruct represents a promising therapeutic approach. The Ru@ACEI platform establishes a foundation for developing multifunctional nanotherapeutics that address the complex pathophysiology of chronic wounds and potentially other oxidative stress-related diseases.

Declarations of Ethics Approval and Consent

All animal procedures were approved by the Animal Ethics Committee of Sun Yat-sen University (approval number: SYSU-IACUC-2025-B2075), and was strictly compliant with the Guide for the Care and Use of Laboratory Animals of the National Institutes of Health.

Author Contributions

Qingyan Li, Weilin Zheng and Jingge Cheng contributed equally to this work. All authors made a significant contribution to the work reported, whether that is in the conception, study design, execution, acquisition of data, analysis and interpretation, or in all these areas; took part in drafting, revising or critically reviewing the article; gave final approval of the version to be published; have agreed on the journal to which the article has been submitted; and agree to be accountable for all aspects of the work.

Funding

This research was supported by "415" Research Project, Emergency Resuscitation Institute (Xiaoxing Liao, ZSQY202341501), Sanming Project of Medicine in Shenzhen Guangming (No.szgmtd2025005), and The Seventh Affiliated Hospital of Sun Yat-sen University (Shenzhen Key Medical Discipline Construction Program Matching Funds, No.00302600004).

Disclosure

The authors declare no competing interests.

References

1. Malone-Povolny MJ, Maloney SE, Schoenfisch MH. Nitric oxide therapy for diabetic wound healing. *Adv Healthc Mater*. 2019;8(12):e1801210. doi:10.1002/adhm.201801210
2. Bugara B, Konieczny P, Wolnicka-Glubisz A, et al. MCPIP1 contributes to the inflammatory response of UVB-treated keratinocytes. *J Dermatol Sci*. 2017;87(1):10–18. doi:10.1016/j.jdermsci.2017.03.013
3. Yang Q, Fang D, Chen J, et al. LncRNAs associated with oxidative stress in diabetic wound healing: regulatory mechanisms and application prospects. *Theranostics*. 2023;13(11):3655–3674. doi:10.7150/thno.85823
4. Guo Y, Ding S, Shang C, et al. Multifunctional PtCuTe nanosheets with strong ROS scavenging and ROS-independent antibacterial properties promote diabetic wound healing. *Adv Mater*. 2024;36(8):e2306292. doi:10.1002/adma.202306292
5. Tu C, Lu H, Zhou T, et al. Promoting the healing of infected diabetic wound by an anti-bacterial and nano-enzyme-containing hydrogel with inflammation-suppressing, ROS-scavenging, oxygen and nitric oxide-generating properties. *Biomaterials*. 2022;286:121597. doi:10.1016/j.biomaterials.2022.121597
6. Guan Y, Niu H, Liu Z, et al. Sustained oxygenation accelerates diabetic wound healing by promoting epithelialization and angiogenesis and decreasing inflammation. *Sci Adv*. 2021;7(35). doi:10.1126/sciadv.abj0153.
7. Yin Z, Wan B, Gong G, Yin J. ROS: executioner of regulating cell death in spinal cord injury. *Front Immunol*. 2024;15:1330678. doi:10.3389/fimmu.2024.1330678
8. Qi X, Li Y, Xiang Y, et al. Hyperthermia-enhanced immunoregulation hydrogel for oxygenation and ROS neutralization in diabetic foot ulcers. *Cell Biomat*. 2025;1(3):100020. doi:10.1016/j.celbio.2025.100020
9. Cheng S, Wang H, Pan X, et al. Dendritic hydrogels with robust inherent antibacterial properties for promoting bacteria-infected wound healing. *ACS Appl Mat Interfaces*. 2022;14(9):11144–11155. doi:10.1021/acsami.1c25014
10. He M, Chen F, Shao D, Weis P, Wei Z, Sun W. Photoresponsive metallopolymer nanoparticles for cancer theranostics. *Biomaterials*. 2021;275:120915. doi:10.1016/j.biomaterials.2021.120915
11. Lu Y, Zhu D, Gui L, et al. A dual-targeting ruthenium nanodrug that inhibits primary tumor growth and lung metastasis via the PARP/ATM pathway. *J Nanobiotechnol*. 2021;19(1):115. doi:10.1186/s12951-021-00799-3
12. Lin P, Qian Z, Liu S, et al. A single-cell RNA sequencing guided multienzymatic hydrogel design for self-regenerative repair in diabetic mandibular defects. *Adv Mater*. 2024;36(50):e2410962. doi:10.1002/adma.202410962

13. Zhang W, Liu W, Long L, et al. Responsive multifunctional hydrogels emulating the chronic wounds healing cascade for skin repair. *J Controlled Release*. 2023;354:821–834. doi:10.1016/j.jconrel.2023.01.049
14. Guo W, Hu C, Wang Y, et al. NO-releasing double-crosslinked responsive hydrogels accelerate the treatment and repair of ischemic stroke. *Acta Pharmaceutica Sinica B*. 2025;15(2):1112–1125. doi:10.1016/j.apsb.2025.01.005
15. Gong H, Yang L, Li Y, et al. Metal-polyphenol nanocomposite hybrid hydrogel: a multifunctional platform for treating diabetic foot ulcers through metabolic microenvironment reprogramming. *Biomaterials*. 2025;322:123414. doi:10.1016/j.biomaterials.2025.123414
16. Yan G, Chang T, Zhao Y, et al. The effects of Ophiocordyceps sinensis combined with ACEI/ARB on diabetic kidney disease: a systematic review and meta-analysis. *Phytomedicine*. 2023;108:154531. doi:10.1016/j.phymed.2022.154531
17. Umanath K, Lewis JB. Update on diabetic nephropathy: core curriculum 2018. *Am J Kidney Dis*. 2018;71(6):884–895. doi:10.1053/j.ajkd.2017.10.026
18. Vaka VR, McMaster KM, Cunningham MW Jr, et al. Role of mitochondrial dysfunction and reactive oxygen species in mediating hypertension in the reduced uterine perfusion pressure rat model of preeclampsia. *Hypertension*. 2018;72(3):703–711. doi:10.1161/HYPERTENSIONAHA.118.11290
19. Cheuy V, Picciolini S, Bedoni M. Progressing the field of regenerative rehabilitation through novel interdisciplinary interaction. *NPJ Regen Med*. 2020;5:16. doi:10.1038/s41536-020-00102-2
20. Xi J, Zhang R, Wang L, et al. A nanozyme-based artificial peroxisome ameliorates hyperuricemia and ischemic stroke. *Adv Funct Mat*. 2021;31(9):2007130. doi:10.1002/adfm.202007130
21. American Diabetes Association Professional Practice Committee. 2. classification and diagnosis of diabetes: standards of medical care in diabetes-2022. *Diabetes Care*. 2022;45(Suppl 1):S17–s38. doi:10.2337/dc22-S002
22. Sm RDD, Tiwari VK, McCune CD, Dhokale RA, Berkowitz DB. Biomacromolecule-assisted screening for reaction discovery and catalyst optimization. *Chem Rev*. 2022;122(16):13800–13880. doi:10.1021/acs.chemrev.2c00213
23. Wang G, Li X, Li N, et al. Icariin alleviates uveitis by targeting peroxiredoxin 3 to modulate retinal microglia M1/M2 phenotypic polarization. *Redox Biol*. 2022;52:102297. doi:10.1016/j.redox.2022.102297
24. Wu J, You K, Chen C, et al. High pretreatment LDH predicts poor prognosis in hypopharyngeal cancer. *Front Oncol*. 2021;11:641682. doi:10.3389/fonc.2021.641682
25. Ghasemi M, Turnbull T, Sebastian S, Kempson I. The MTT assay: utility, limitations, pitfalls, and interpretation in bulk and single-cell analysis. *Int J Mol Sci*. 2021;22(23):12827. doi:10.3390/ijms222312827
26. He S, Li Z, Wang L, et al. A nanoenzyme-modified hydrogel targets macrophage reprogramming-angiogenesis crosstalk to boost diabetic wound repair. *Bioact Mater*. 2024;35:17–30. doi:10.1016/j.bioactmat.2024.01.005
27. Zhou F, Gao H, Shang L, et al. Oridonin promotes endoplasmic reticulum stress via TP53-repressed TCF4 transactivation in colorectal cancer. *J Exp Clin Cancer Res*. 2023;42(1):150. doi:10.1186/s13046-023-02702-4
28. Zhong J, Mao X, Li H, et al. Single-cell RNA sequencing analysis reveals the relationship of bone marrow and osteopenia in STZ-induced type 1 diabetic mice. *J Adv Res*. 2022;41:145–158. doi:10.1016/j.jare.2022.01.006
29. Ansari MY, Novak K, Haqqi TM. ERK1/2-mediated activation of DRP1 regulates mitochondrial dynamics and apoptosis in chondrocytes. *Osteoarthritis Cartilage*. 2022;30(2):315–328. doi:10.1016/j.joca.2021.11.003
30. de Haan K, Zhang Y, Zuckerman JE, et al. Deep learning-based transformation of H&E stained tissues into special stains. *Nat Commun*. 2021;12(1):4884. doi:10.1038/s41467-021-25221-2
31. Kim BK, Lee SA, Park M, et al. Ultrafast real-time PCR in photothermal microparticles. *ACS Nano*. 2022;16(12):20533–20544. doi:10.1021/acsnano.2c07017
32. Manciu M, Manciu FS, Ruckenstein E. On the surface tension and Zeta potential of electrolyte solutions. *Adv Colloid Interface Sci*. 2017;244:90–99. doi:10.1016/j.cis.2016.06.006
33. Michaeloudes C, Abubakar-Waziri H, Lakhdar R, et al. Molecular mechanisms of oxidative stress in asthma. *Mol Aspects Med*. 2022;85:101026. doi:10.1016/j.mam.2021.101026
34. Steinberg SF. Oxidative stress and sarcomeric proteins. *Circ Res*. 2013;112(2):393–405. doi:10.1161/CIRCRESAHA.111.300496
35. Chi C, Fu H, Li YH, et al. Exerkine fibronectin type-III domain-containing protein 5/irisin-enriched extracellular vesicles delay vascular ageing by increasing SIRT6 stability. *Eur Heart J*. 2022;43(43):4579–4595. doi:10.1093/eurheartj/ehac431
36. Li J, Zhang J, Yu P, et al. ROS-responsive & scavenging NO nanomedicine for vascular diseases treatment by inhibiting endoplasmic reticulum stress and improving NO bioavailability. *Bioact Mater*. 2024;37:239–252. doi:10.1016/j.bioactmat.2024.03.010